Proceedings of the Fifteenth International Conference on
Computational Structures Technology
Edited by: P. Iványi, J. Kruis and B.H.V. Topping
Civil-Comp Conferences, Volume 9, Paper 14.3
Civil-Comp Press, Edinburgh, United Kingdom, 2024
ISSN: 2753-3239, doi: 10.4203/ccc.9.14.3

Blast Responses of a Reinforced Concrete Slab Using the Arbitrary Lagrangian-Eulerian Method

T. H. Lee, D. Park, Y. Choi, Y. Lee and J.-W. Hong

Department of Civil and Environmental Engineering, KAIST, Republic of Korea

Abstract

Numerical simulation emerges as a highly effective method for studying the interaction between structures and blast waves. In this study, we apply a multi-material arbitrary Lagrangian-Eulerian method to explore the dynamic response of a reinforced concrete slab under explosion load. The Arbitrary Lagrangian-Eulerian method is a finite element method in fluid and solid mechanics to simulate complicated interactions of solids and fluids. The numerical model is validated by comparing the maximum reflected pressure and mid-span deflection with the results from blast experiments on reinforced concrete slab. In addition, damage patterns in the slab are analyzed using the validated model. This effective modeling technique will be highly useful in the design of infrastructure to enhance blast resistance.

Keywords: blast, reinforced concrete slab, arbitrary Lagrangian-Eulerian method, finite element analysis, dynamic response, blast resistance.

1 Introduction

Understanding the interaction between blast and structural members has been considered crucial in design, protection, and reinforcement of infrastructures due to the increasing possibility of explosions by accidents and terrorist attacks. Reinforced concrete (RC) slab, favored for its strength and flexibility under various stresses, is widely used in the construction of essential infrastructure, and it is essential to assess the response of RC slabs to explosions to ensure structural integrity and safety. However, traditional experimental approaches to studying the blast response of RC slab have limitations due to environmental degradation, high costs, and difficulty of observation. Simulation can be an effective alternative because it can provide time-domain responses to blast waves, and the methodology takes much less costs than experiments.

To analyze the effects of blast loading on RC slabs, it is crucial to consider nonlinear fluid dynamics, structural mechanics, and fluid-structure interactions. Unlike structure-structure contact, fluid-structure contact may cause significant mesh distortion, especially at the fluid-structure interface. Here, a fluid element might become so distorted that its volume is calculated as negative, leading to premature termination of the computation. Avoiding fluid mesh distortion in fluid-structure applications, the fluid is modeled using a multi-material arbitrary Lagrangian-Eulerian (MM-ALE) formulation. This method is validated for several applications [1–8].

In this paper, we utilize MM-ALE to model an RC slab in an airburst and present the structural dynamic responses to blast loading. The governing equations of the ALE formulation are described, and the advection algorithms for solving mass, momentum, and energy conservation within the multi-material formulation are discussed. The accuracy of the numerical model is verified by comparing blast pressure and mid-span deflection with experimental results from field blast tests documented in the literature. Additionally, damage patterns are investigated to identify the failure mechanism of the RC slab under blast loading. This research paves the way for the development of structures more resistant to blasts, enhancing their ability to withstand extreme conditions and significantly contributing to the field of structural engineering.

2 Theory

2.1 ALE multi-material formulation

In the ALE formulation, a reference coordinate that is not the Lagrangian coordinate and Eulerian coordinate is induced [9]. The differential quotient relating the material to this reference coordinate system is given as

$$\frac{\partial f(X_i,t)}{\partial t} = \frac{\partial f(x_i,t)}{\partial t} + w_i \frac{\partial f(x_i,t)}{\partial x_i}, \tag{1}$$

where X_i are the Lagrangian coordinates, x_i are the Eulerian coordinates, and w_i are the relative velocities of material to mesh. Therefore, the ALE formulation can be derived from the relationship between the time derivative of the material and that of the reference geometry configuration [10].

2.2 Conservation equations

The governing equations in the fluid domain consist of the mass conservation equation, momentum conservation equation, and energy conservation equation [11]. These three conservation equations are utilized to calculate the velocities and displacements of both elements and the materials. The governing equations are expressed as

$$\frac{\partial \rho}{\partial t} = -\rho \frac{\partial v_i}{\partial x_i} - w_i \frac{\partial \rho}{\partial x_i}, \tag{2}$$

$$\rho \frac{\partial v_i}{\partial t} = \sigma_{ij,j} + \rho b_i - \rho w_i \frac{\partial v_i}{\partial x_j}, \tag{3}$$

$$\rho \frac{\partial E}{\partial t} = \sigma_{ij} v_{i,j} + \rho b_i v_i - \rho w_j \frac{\partial E}{\partial x_j}, \tag{4}$$

where ρ represents the material density, x_i are displacements, v_i are velocities of the material, w_i are the relative velocities, σ_{ij} are stresses, b_i are the volumetric forces that act on the mass of the fluid elements, and E denotes the energy. The stress tensor can be written as

$$\sigma_{ij} = -p\delta_{ij} + \mu(v_{i,j} + v_{j,i}), \tag{5}$$

where δ_{ij} is the Kronecker delta function, p is the pressure within the fluid, and μ represents the dynamic viscosity.

In the ALE multi-material formulation, the detached operator method is employed, wherein the calculation at each time step is divided into two parts to solve the ALE equation [12]. Initially, the Lagrangian approach is applied, by moving the mesh together with the material. During this phase, the equilibrium equations are described as

$$\rho \frac{\partial v_i}{\partial t} = \sigma_{ij,j} + \rho b_i, \tag{6}$$

$$\rho \frac{\partial E}{\partial t} = \sigma_{ij} v_{i,j} + \rho b_i v_i, \tag{7}$$

In the Lagrangian phase, material does not flow across the element boundaries, ensuring compliance with mass conservation. In the second stage, the transported volume, internal energy, and kinetic energy of materials flowing through the boundaries are calculated. At this stage, the meshes are remapped to their initial or arbitrary positions. For each node, the velocity vector $\mathbf{u}$ and displacement vector $\mathbf{x}$ are updated according to the following equations:

$$\mathbf{u}^{n+\frac{1}{2}} = \mathbf{u}^{n-\frac{1}{2}} + \Delta t \mathbf{M}^{-1}(\mathbf{F}^n_{ext} + \mathbf{F}^n_{int}), \tag{8}$$

$$\mathbf{x}^{n+1} = \mathbf{x}^{n-1} + \Delta t \mathbf{u}^{n+\frac{1}{2}}, \tag{9}$$

where $\mathbf{M}$ is a diagonal mass matrix, $\mathbf{F}_{ext}^{n}$ represents the vector of external force, and $\mathbf{F}_{int}^{n}$ is the vector of internal force.

2.3 Fluid-structure-coupling algorithm

In an explicit time integration, modal forces for both fluid and structure, along with coupling forces at the fluid-structure interface, are calculated within the time step. For each structure node, the depth penetration vector $\mathbf{d}$ is incrementally updated at each time step [13]. This update uses the relative velocities at the slave node to the master node. At time $t = t^n$, the depth penetration vector $\mathbf{d}^n$ is updated by

$$\mathbf{d}^{n+1} = \mathbf{d}^{n} + \left(\mathbf{v}_s^{n+\frac{1}{2}} - \mathbf{v}_f^{n+\frac{1}{2}} \right) \Delta t, \tag{10}$$

where Δt denotes the increment of time, $\mathbf{v}_s$ is the structure velocity at the slave node, and $\mathbf{v}_f$ is the fluid velocity at the master node's location, interpolated from the fluid element's nodes at the current time. The vector $\mathbf{d}^n$ represents the penetration of the structure inside the fluid during the time step [14]. The coupling force is applied only if penetration occurs. The penalty coupling functions are calculated in proportion to the penetration depth and the stiffness of the spring. The head of the spring is connected to the structure at the slave node, while the tail of the spring is connected to the master node within a fluid element that is intersected by the structure [15]. The coupling force is written as

$$\mathbf{F} = k\mathbf{d}, \tag{11}$$

where k denotes the stiffness of the spring. The coupling force $\mathbf{F}$ is applied in opposite directions to both the master and slave nodes at the coupling interface, and the stiffness is calculated as [16]

$$k = p_f \frac{KA}{V}. \tag{12}$$

The spring stiffness is derived from the explicit penalty contact algorithm used in LS-DYNA [9]. Numerical stiffness per unit area is expressed based on the bulk modulus K of the fluid element involved in coupling with the slave structure node, the volume V of the fluid element containing the master fluid node, and the average area A of the structure elements connected to the structure node [13]. To prevent numerical instabilities, a penalty factor $0 \leq p_f \leq 1$ is introduced to adjust the calculated stiffness of the interacting system.

3 Description of the finite element model

3.1 Field blast test from literature

The numerical model is constructed based on field blast tests in Ref. [17]. Figure 1 shows the test configuration and cross-sectional views of the slab specimens. The dimensions of the slab were $1000 \times 1100 \times 40\ \mathrm{mm}^3$. A single layer of reinforcing rebars were positioned near the slab's bottom face, featuring steel rebars having a 6 mm diameter. These rebars featured an elastic modulus of 210 GPa and a yield strength of 534 MPa. The spacing between the rebars was 75 mm. The slab was supported by a steel frame, spanning 1,000 mm. TNT was used as the explosive charge, characterized by a detonation velocity of 6,730 m/s and density of $1.6\ \mathrm{g/cm}^3$. The distance between the explosive charge and the slab surface was consistently maintained at 400 mm. The explosive, a cubic weighing 400 g measured $63.0 \times 126.0 \times 31.5\ \mathrm{mm}^3$. During the experiments, the maximum explosive overpressure was measured by a pressure sensor placed at the edge of the slab. Additionally, a linear variable displacement transformer (LVDT) was positioned below the center of the slab to measure the maximum mid-span deflection, indicating the vertical displacement at the center of the structure. Detailed information on the experimental procedure is available in Ref. [17].

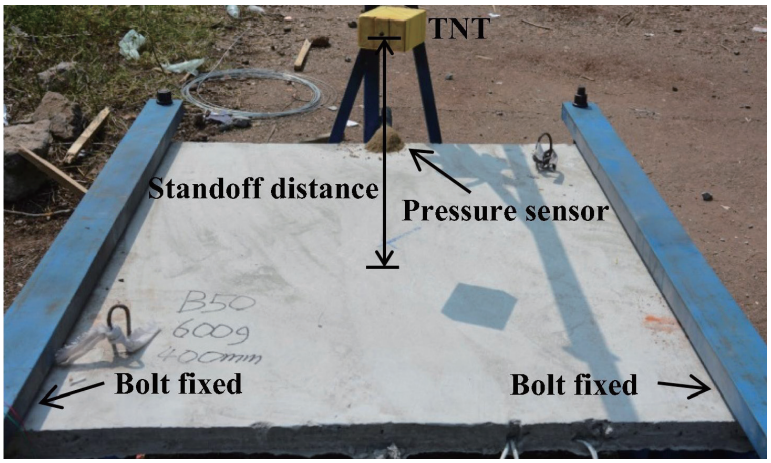

Figure 1: Experiemnt setup for blast test [17].

3.2 Numerical blast model

Figure 2 shows the configuration of the numerical model based on the field test setup. The concrete part is modeled using 3D Lagrangian 8-node hexahedral elements, while the reinforcing mesh component employs 2D beam elements. Instead of sharing nodes, constraints are applied between beams and solids to synchronize their movement, thereby simulating a reinforced concrete structure. The support component is also comprised of 3D Lagrangian elements, with its nodes fixed in all directions. To simulate the nonlinear behavior of a concrete structure during an explosion, we use the

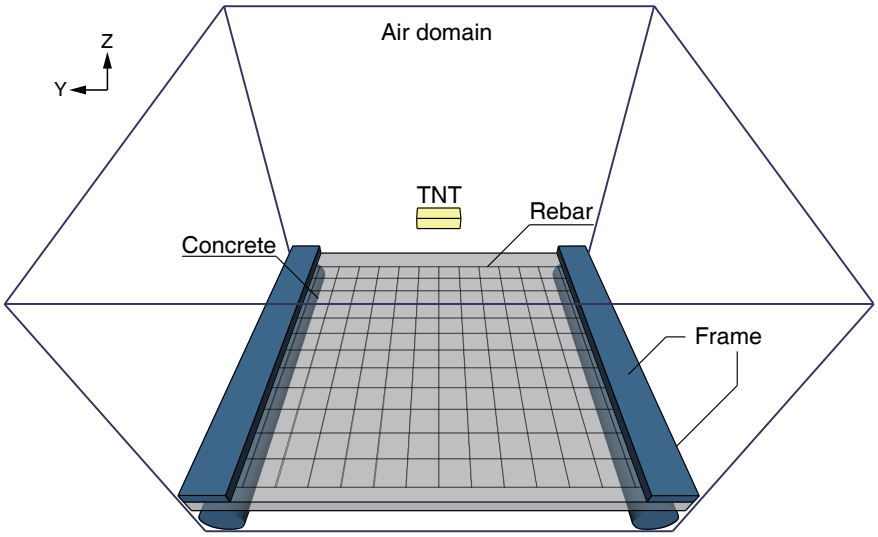

Figure 2: Geometrical model description.

continuous surface cap model (CSCM). The rebar and steel frame parts are modeled by using the bilinear elastic-plastic model (MAT 3), which is widely employed to simulate isotropic and kinematic hardening plasticity [18]. The air domain is discretized using hexahedron elements to surround both a reinforced concrete slab and TNT. The volume fraction and locations of the two materials in the ALE mesh are defined separately [19]. The explosive is modeled using LS-DYNA's high explosive burm material model and the Jones-Wilkins-Lee (JWL) equation of state (EOS), which defines denotation pressure as a function of the detonation product's relative volume and the initial internal energy of the explosive. Air is modeled as an ideal gas [20], employing the null material model with a polynomial EOS to describe the relationship between internal energy and pressure. The properties of the materials for both fluids and structures are detailed in Table 1.

Componenet	Property	
Slab	Density (kg/m^3)	2,400
	Compressive strength (MPa)	46.9
Rebar, steel frame	Density (kg/m^3)	7,800
	Young's modulus (GPa)	210
	Poisson's ratio	0.3
	Yield strength (MPa)	534
Air	Density (kg/m^3)	1.25
TNT	Density (kg/m^3)	1,600
	Detonation velocity (m/s)	6,930
	Chapman-Jouget pressure (GPa)	21.0

Table 1: Material properties [17].

4 Simulation results

The comparison of numerical and experimental results are carried out by investigating the time histories of blast overpressure and mid-span deflection of the RC slab, as shown in Figure 3-(a) and (b). The numerical results demonstrate good agreement with the experimental data concerning peak pressure, exhibiting an error of lower than 10%, and mid-span deflection, showing an error of lower than 5%.

Consequently, the numerical model of blast simulation using the MM-ALE method reliably reflects the intended blast behavior from the experimental results. The failure

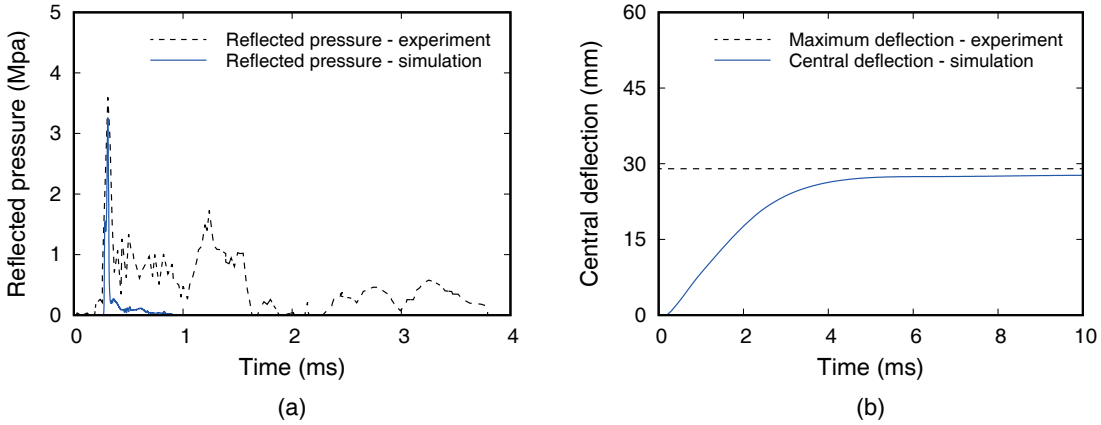

Figure 3: Comparison of the field blast test and simulation results: (a) time histories of the blast pressure and (b) mid-span deflection.

mechanism of the structure to the blast wave on a microscopic time scale is analyzed by investigating the numerical results. The damage pattern of the RC slab, as observed experimentally, along with the numerical results of structural failure at 10 ms, are presented in Figure 4. The damage represents the crack propagation in concrete. A value of 0 for the damage parameter indicates that the element is undamaged, whereas the value of 1 signifies complete failure. When the slab is subjected to blast loading, tension occurs on the bottom surface, while the top surface undergoes compression. Due to concrete being much more sensitive to tension than to compression, minor cracks initially appear on the bottom surface. These cracks subsequently develop into eminent radial cracks. Damage on the bottom surface intensifies, especially at the center, and a black area indicative of scabbing is observed on the bottom surface.

5 Conclusion

In this study, we employ the MM-ALE method to model the dynamic response of reinforced concrete (RC) slabs under blast loading conditions. By comparing the numerical simulations with experimental data, we validate the accuracy and reliability of the numerical methodology, particularly in simulating the reflected peak pressure and mid-span deflection. The damage patterns from the validated model are also analyzed

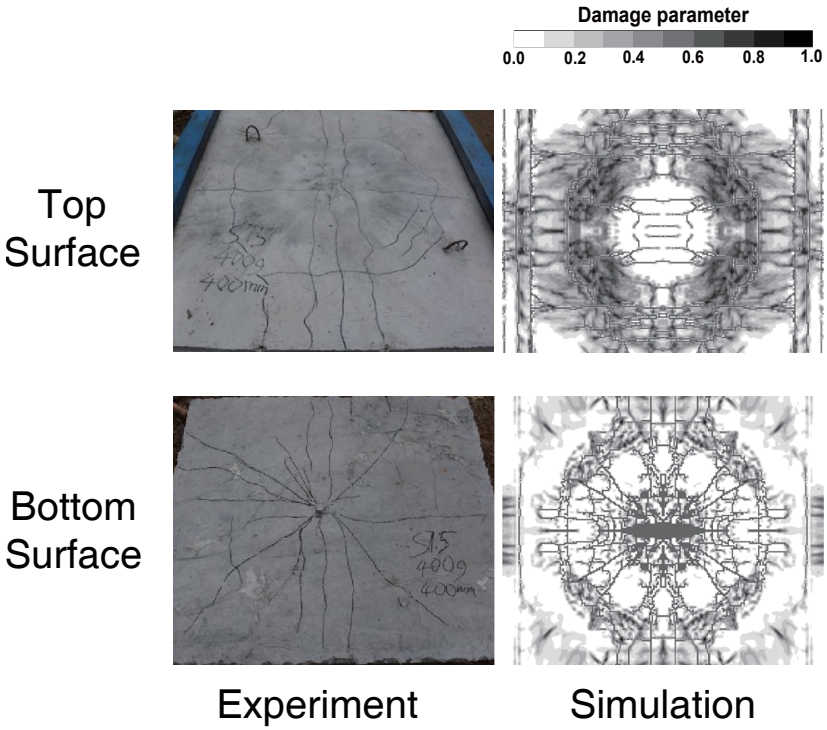

Figure 4: Surface damage patterns of the field blast test and simulation results.

to identify the failure mechanism of the RC slab under blast loading. The simulation results highlight the accuracy of the MM-ALE method in simulating the complicated interactions between blast waves and structural elements. In future work, we plan to analyze the more comprehensive failure mechanism of RC slabs based on a validated numerical model in various blast scenarios. This prospective research will expand the understanding of structural responses under extreme loading conditions.

Acknowledgments

This work was supported by the Nuclear Safety Research Program through the Korea Foundation Of Nuclear Safety(KoFONS) using the financial resource granted by the Nuclear Safety and Security Commission(NSSC) of the Republic of Korea. (No. 00242257)

References

[1] H.A. Khawaja, R. Messahel, B. Ewan, S. Mhamed, & M. Moatamedi, "Experimental and numerical study of pressure in a shock tube," Journal of Pressure Vessel Technology, 138, 041301, 2016.

[2] M. U. Khan, M. Moatamedi, M. Souli, & T. Zeguer, "Multiphysics out of position airbag simulation," International journal of crashworthiness, 13, 159-166, 2008.
[3] Z. Ozdemir, M. Souli, & M. F. Yasin, "Numerical evaluation of nonlinear response of broad cylindrical steel tanks under multidimensional earthquake motion," Earthquake spectra, 28, 217-238, 2012.
[4] M. Souli, A. V. Kultsep, E. Al-Bahkali, C. C. Pain, & M. Moatamedi, "Arbitrary Lagrangian Eulerian formulation for sloshing tank analysis in nuclear engineering," Nuclear Science and Engineering, 183, 126-134, 2016.
[5] R. Messahel, B. Cohen, M. Souli, & M. Moatammedi, "Fluid-structure interaction for water hammers effects in petroleum and nuclear plants," The International Journal of Multiphysics, 5, 377-386, 2011.
[6] R. Messahel, B. Cohen, M. Moatamedi, A. Boudlal, M. Souli, & N. Aquelet, "Numerical and experimental investigations of water hammers in nuclear industry," The International Journal of Multiphysics, 9, 21-36, 2015.
[7] M. Moatamedi, M. Souli, & E. Al-Bahkali, "Fluid structure modelling of blood flow in vessels," Molecular & Cellular Biomechanics, 11, 221, 2014.
[8] S. Mhamed, A. B. Essam, A. B. Thamer, & M. Mojtaba, "Investigation of blood flow modeling in artery using ALE formulation," International Journal of Computational Methods, 14, 1750001, 2017.
[9] S. Wang, & C. G. Soares, "Numerical study on the water impact of 3D bodies by an explicit finite element method," Ocean Engineering, 78, 73-88, 2014.
[10] S. Wang, & C. G. Soares, "Slam induced loads on bow-flared sections with various roll angles," Ocean Engineering, 67, 45-57, 2013.
[11] H. Louahlia-Gualous, & M. Asbik, "Numerical modeling of annular film condensation inside a miniature tube," Numerical Heat Transfer, Part A: Applications, 52, 251-273, 2007.
[12] M. Souli, & I. Shahrour, "A coupling method for soil structure interaction problems," International Journal for Numerical and Analytical Methods in Geomechanics, 37, 1140-1153, 2013.
[13] N. Aquelet, M. Souli, & L. Olovsson, "Euler-Lagrange coupling with damping effects: Application to slamming problems," Computer methods in applied mechanics and engineering, 195, 110-132, 2006.
[14] B. Yang, G. Zhang, Z. Huang, Z. Sun, & Z. Zong, "Numerical simulation of the ice resistance in pack ice conditions," International Journal of Computational Methods, 17, 1844005, 2020.
[15] Y. Shi, G. Pan, S. C. Yim, G. Yan, & D. Zhang, "Numerical investigation of hydroelastic water-entry impact dynamics of AUVs," Journal of Fluids and Structures, 91, 102760, 2019.
[16] Y. Shi, G. Pan, G. X. Yan, S. C. Yim, & J. Jiang, "Numerical study on the cavity characteristics and impact loads of AUV water entry," Applied Ocean Research, 89, 44-58, 2019.
[17] J. Feng, Y. Zhou, P. Wang, B. Wang, J. Zhou, H. Chen, H. Fan, F. Jin, "Experimental research on blast-resistance of one-way concrete slabs reinforced by

BFRP bars under close-in explosion," Engineering Structures, 150, 550-561, 2017.

[18] K. Ko, S. Jin, S. E. Lee, & J. W. Hong, "Impact resistance of nacre-like composites diversely patterned by 3D printing," Composite Structures, 238, 111951, 2020.

[19] LSTC, "LS-DYNA User's Manual—Version R 11.0," Livermore Software Technology Corporation Livermore, CA, 2017.

[20] Z. L. Wang, Y. C. Li, & R. F. Shen, "Numerical simulation of tensile damage and blast crater in brittle rock due to underground explosion," International Journal of Rock Mechanics and Mining Sciences, 44(5), 730-738, 2007.